Structure
Article

Structural Basis of the Initial Binding of tRNA^{Ile} Lysidine Synthetase TilS with ATP and L-Lysine

Mitsuo Kuratani,[1,2] Yuka Yoshikawa,[3] Yoshitaka Bessho,[2] Kyoko Higashijima,[2] Takeshi Ishii,[2] Rie Shibata,[2] Seizo Takahashi,[3] Katsuhide Yutani,[4] and Shigeyuki Yokoyama[1,2,4,*]
[1]Department of Biophysics and Biochemistry, Graduate School of Science, The University of Tokyo, 7-3-1 Hongo, Bunkyo-ku, Tokyo 113-0033, Japan
[2]Genomic Sciences Center, Yokohama Institute, RIKEN, 1-7-22 Suehiro-cho, Tsurumi, Yokohama, 230-0045, Japan
[3]Faculty of Science, Japan Women's University, Tokyo 112-0015, Japan
[4]RIKEN Harima Institute at SPring-8, 1-1-1 Kouto, Mikazuki-cho, Sayo-gun, Hyogo 679-5148, Japan
*Correspondence: yokoyama@biochem.s.u-tokyo.ac.jp
DOI 10.1016/j.str.2007.09.020

SUMMARY

In the bacterial genetic-code system, the codon AUA is decoded as isoleucine by tRNA$^{Ile}_2$ with the lysidine residue at the wobble position. Lysidine is derived from cytidine, with ATP and L-lysine, by tRNA^{Ile} lysidine synthetase (TilS), which is an N-type ATP pyrophosphatase. In this study, we determined the crystal structure of *Aquifex aeolicus* TilS, complexed with ATP, Mg^{2+}, and L-lysine, at 2.5 Å resolution. The presence of the TilS-specific subdomain causes the active site to have two separate gateways, a large hole and a narrow tunnel on the opposite side. ATP is bound inside the hole, and L-lysine is bound at the entrance of the tunnel. The conserved Asp36 in the PP-motif coordinates Mg^{2+}. In these initial binding modes, the ATP, Mg^{2+}, and L-lysine are held far apart from each other, but they seem to be brought together for the reaction upon cytidine binding, with putative structural changes of the complex.

INTRODUCTION

The first base of the tRNA anticodon (position 34 or the wobble position) base pairs with the third base of the codon and plays a pivotal role in translation. Numerous posttranscriptional modifications are present at position 34, and these maintain precise decoding by fine tuning the base pairing properties (Agris et al., 2007; Bjork and Hagervall, 2005; Crick, 1966; Marck and Grosjean, 2002; Suzuki, 2005; Yokoyama and Nishimura, 1995). Lysidine (2-lysyl cytidine; abbreviated as L or k^2C) is a modified cytidine present at position 34 of the bacterial AUA codon specific tRNA$^{Ile}_2$, and it pairs with adenosine instead of guanosine (Muramatsu et al., 1988a, 1988b). Lysidine is introduced by tRNA^{Ile} lysidine synthetase (TilS) (Soma et al., 2003) in all bacteria harboring tRNA^{Ile} (CAT) genes. An exception is found in *Mycoplasma mobile*, which has a tRNA^{Ile} (TAT) gene instead (Silva et al., 2006). tRNA$^{Ile}_2$ bearing unmodified cytidine at position 34 is charged with methionine by methionyl-tRNA synthetase (MetRS) and deciphers the AUG methionine codon (Muramatsu et al., 1988a; Soma et al., 2003). Lysidine introduction to tRNA$^{Ile}_2$ prevents the MetRS binding while it accepts isoleucine attachment by isoleucyl-tRNA synthetase (IleRS). Thus, the lysidine modification converts the base-pairing property as well as the amino acid specificity of tRNA$^{Ile}_2$, which is necessary for the translation of the isoleucine AUA codon to maintain the bacterial genetic code (Muramatsu et al., 1988a; Soma et al., 2003). On the other hand, eukaryotes use tRNA^{Ile} (IAU) for reading the isoleucine AUA codon (Gerber and Keller, 1999; Marck and Grosjean, 2002), and thus a new antibiotic could be developed by inhibiting lysidine formation.

Lysidine formation proceeds in two consecutive reactions (Ikeuchi et al., 2005). The α phosphate of ATP is first attached to the cytidine residue to form an intermediate adenylated cytidine and a pyrophosphate (Figure 1), and the subsequent nucleophilic attack by L-lysine on the adenylated cytidine completes the reaction (Figure 1). TilS belongs to the N-type ATP pyrophosphatase family, which commonly utilizes ATP and a nitrogen nucleophile, and has the signature PP-motif (SGGxDS) (Bork and Koonin, 1994). The PP-motif is involved in binding to the β and γ phosphates of ATP (Lemke and Howell, 2001; Tesmer et al., 1996). In addition, a second weakly conserved motif of TilS (PLxxxxK/R) was proposed to be involved in the γ phosphate recognition (Ikeuchi et al., 2005).

The structures of the ligand-free form of TilS from *Escherichia coli* (PDB code: 1NI5) and *Aquifex aeolicus* (PDB code: 1WY5) (Nakanishi et al., 2005) were determined. However, no structure in a complex with its ligand has been solved. On the other hand, the structure(s) of other N-type ATP pyrophosphatases, containing ATP, AMPPNP, and/or AMP, are available for argininosuccinate synthetase (Goto et al., 2002, 2003; Lemke and Howell, 2001, 2002), NAD^+ synthetase (Rizzi et al., 1998), and GMP synthetase (Tesmer et al., 1996). A docking model

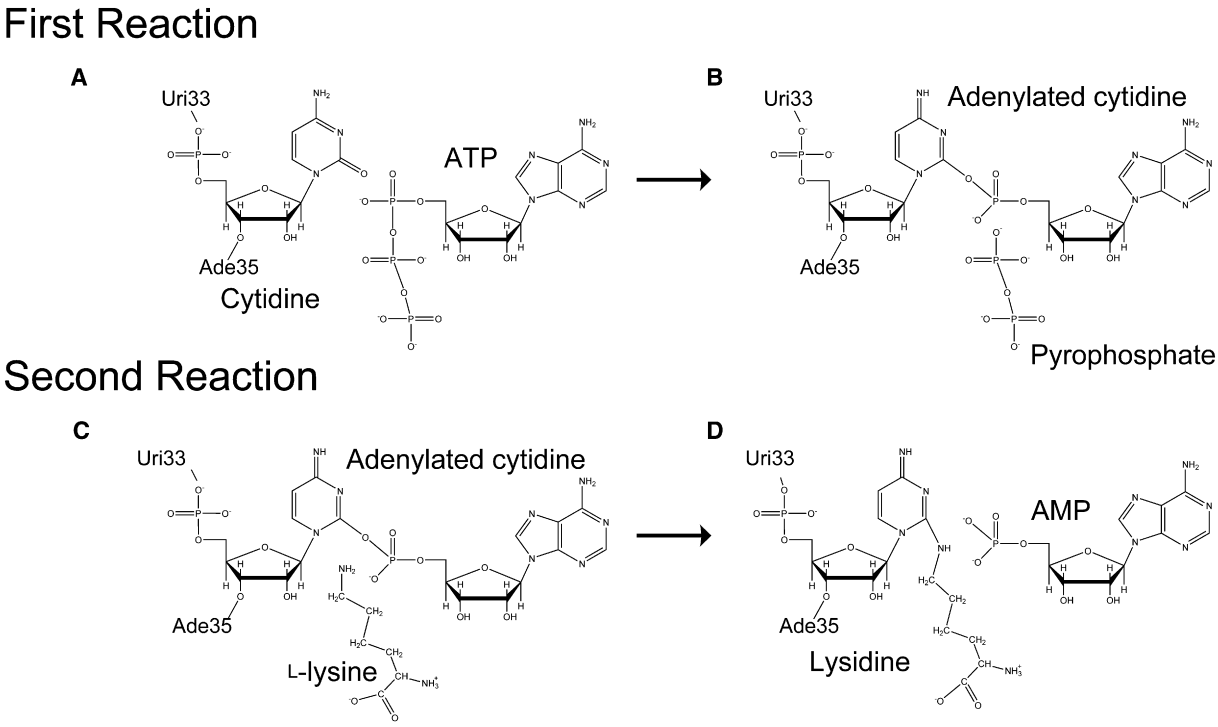

Figure 1. Two-Step Reaction of the Lysidine Synthesis
In the first reaction (A and B), the cytidine residue and ATP react each other to form an intermediate adenylated cytidine and a pyrophosphate. In the second reaction (C and D), L-lysine attacks the adenylated cytidine to produce lysidine and AMP.

and mutational studies of TilS revealed several amino acid residues essential for catalysis (Nakanishi et al., 2005).

In the present study, we determined two crystal structures of *A. aeolicus* TilS, complexed with ATP, Mg^{2+}, and L-lysine and with AMPPNP alone. During the structure determination, we unexpectedly revealed the presence of a disulfide bond in *A. aeolicus* TilS. Conventionally, disulfide bonds in a reducing cytosolic environment were considered to be only marginally stable. However, in some thermophilic organisms, evidence for the presence of disulfide bonds in cytosolic proteins is becoming more and more solid. A survey of the PDB entries revealed that disulfide bonds are rich in the proteins from several thermophilic organisms, as compared to those from mesophilic organisms, which is also supported by comparisons of the cysteine content in the proteins (Beeby et al., 2005; Mallick et al., 2002; Vieille and Zeikus, 2001). Moreover, the disulfide-rich thermophilic organisms contain unique PDO proteins, which would work as a cytosolic disulfide isomerase (Beeby et al., 2005; Pedone et al., 2006). The structural role of the disulfide bond in protein stabilization was verified biochemically, by using an *A. aeolicus* protein (Meyer et al., 2002) as well as archaeal proteins (DeDecker et al., 1996; Karlstrom et al., 2005; Toth et al., 2000). *A. aeolicus* is an aerobic thermophilic bacterium with growth-temperature maxima near 95°C (Deckert et al., 1998), and it has a PDO protein, indicating that disulfide bonds are maintained in the endogenous cytosolic proteins. Therefore, we quantified how this disulfide bond stabilizes the *A. aeolicus* TilS protein by differential scanning calorimetry (DSC). We report here the initial binding mode of TilS with ATP, Mg^{2+}, and L-lysine, as well as the anticipated conformational changes accompanying lysidine synthesis, based on structural comparisons with the substrate-free forms of TilS and with other N-type ATP pyrophosphatases.

RESULTS

Structure Determination

At first, we determined the structure of *A. aeolicus* TilS complexed with AMPPNP (Figure 2A), an ATP analog, at 2.7 Å resolution, with final R and R_{free} factors of 22.6% and 29.4%, respectively (Table 1). The crystal of TilS/AMPPNP contains two homodimers, A-B and C-D, in the asymmetric unit, and two AMPPNP in molecules A and C. However, no electron densities were observed for AMPPNP in molecules B and D.

Next, by increasing the concentrations of ATP and L-lysine during crystallization, we made a cocrystal and determined the structure of *A. aeolicus* TilS complexed with ATP (Figure 2B) and L-lysine (Figure 2C) at 2.5 Å resolution, with final R and R_{free} factors of 22.9% and 27.4%, respectively (Table 1). The crystal contains two homodimers, A-B and C-D, in the asymmetric unit (Figure 2D). Molecule A includes all residues (1–317), whereas molecules B–D lack three or four residues at the C terminus. A strong spherical electron density, corresponding to

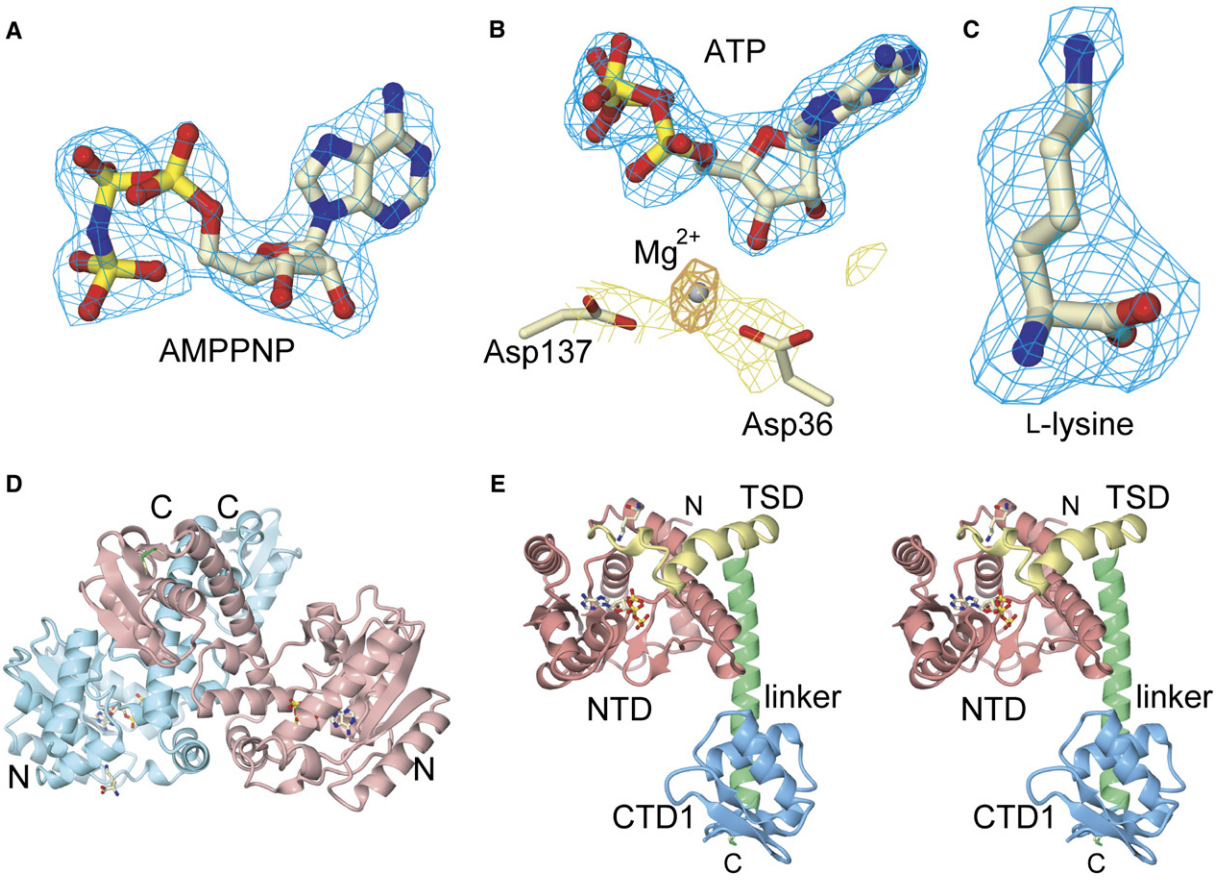

Figure 2. Overall Structure

(A–C) $|Fo| - |Fc|$ simulated annealing omit maps. (A) The electron density of the AMPPNP (blue, contoured at 4σ). (B) The electron densities of the ATP (blue, 5.5σ) and the Mg^{2+} (brown, 4σ). The continuity of the electron densities of the Mg^{2+}, Asp36, and Asp137 is shown by omitting these three molecules (yellow, 3σ). (C) The electron densities of the L-lysine (blue, 3.5σ).

(D) Ribbon model of the TilS dimer. Two subunits (molecules A and B of TilS/ATP/Mg/Lys) are colored pink and cyan, respectively. The ATP and L-lysine molecules are shown by stick models.

(E) A stereoview of the TilS monomer (molecule B of TilS/ATP/Mg/Lys). The N-terminal domain (NTD), the TilS-specific subdomain (TSD), the linker, and the C-terminal domain (CTD1) are colored pink, yellow, green, and cyan, respectively. The graphic figures in this paper were prepared with CueMol (http://cuemol.sourceforge.jp/en/) and were rendered with POVRAY (http://www.povray.org/).

one Mg^{2+}, was located between the two negatively charged aspartic acid residues (Figure 2B). The asymmetric unit contains four ATP molecules, one Mg^{2+} (Figure 2B), and one L-lysine (Figure 2C) in the TilS/ATP/Mg/Lys structure. The amino and carboxyl atoms of the L-lysine interact with the side chains of the other dimer, which is considered to be due to the crystal packing. The structures of TilS/AMPPNP and TilS/ATP/Mg/Lys are considered to be essentially identical, with an average root mean square deviation of 0.67 Å over 1258 C_α atoms. The biological discoveries mainly rely on the structure of TilS/ATP/Mg/Lys, since the resolution is superior, but the TilS/AMPPNP structure revealed that the conformations between ATP and AMPPNP slightly differ, with varied hydrogen bonds with TilS, due to the substitution of the oxygen atom, between the P_β and P_γ atoms in the ATP, by the nitrogen atom in the AMPPNP.

Besides identifying the residues that interact with the substrates, our substrate-bound TilS/ATP/Mg/Lys structure has two other differences as compared to the substrate-free form (1WY5) (Nakanishi et al., 2005). One is that our structure include six residues at the C terminus (^{312}CFSPEV^{317}) (Figure 3), which are absent in 1WY5. These residues revealed that each molecule contains one disulfide bond between Cys253 and Cys312. The second difference is the conformation of residues 190–200, which are unique to TilS among the N-type ATP pyrophosphatases, and are located near the active site.

Monomer Architecture

The *A. aeolicus* TilS monomer (Figure 2E) consists of the conserved N-terminal domain (NTD; residues 1–217), a helix linker, and a C-terminal domain (CTD1; residues 249–317). The *A. aeolicus* TilS contains only CTD1, whereas those from *E. coli* and other species consist of two C-terminal domains, CTD1 and CTD2. The NTD is globular, comprising ten α helices and six β strands, and shares similarities with several ATP pyrophosphatases, including

Table 1. Data Collection and Refinement Statistics

Data Collection Statistics	TilS/AMPPNP	TilS/ATP/Mg/Lys
Wavelength (Å)	1.0000	1.0000
Resolution (Å)	50–2.7 (2.8–2.7)	50–2.5 (2.59–2.5)
Unique Reflections	46,600	52,465
Redundancy	4.1 (3.8)	2.6 (1.7)
Completeness (%)	99.4 (96.5)	91.8 (78.0)
I/σ (I)	13.3 (1.8)	12.3 (2.3)
R_{sym} (%)	8.8 (44.2)	8.4 (22.1)
Refinement Statistics		
Resolution (Å)	2.7	2.5
Reflections (σ (F) > 0)	46,266	52.457
Number of protein atoms	10,447	10,442
Water atoms	180	65
AMPPNP molecules	2	
ATP molecules		4
Magnesium ion		1
L-lysine		1
R_{work} factor (%)	22.6	22.9
R_{free} factor (%)	29.4	27.4
Rmsd bond length (Å)	0.009	0.014
Rmsd bond angles (deg)	1.4	1.7
Average B factor (Å^2)		
Protein atoms	53.4	54.3
Water atoms	34.0	38.0
Ramachandran Plot		
Most favored (%)	85.6	86.1
Additional allowed (%)	13.2	12.5
Generously allowed (%)	1.2	1.4

$R_{sym} = \Sigma_{hkl} \Sigma_j | I_j(hkl) - < I_j(hkl) > | / \Sigma_{hkl} \Sigma_j I(hkl)$, where $I_j(hkl)$ and $< I_j(hkl) >$ are the intensity of measurement j and the mean intensity for the reflection with indices hkl, respectively. R factor = $\Sigma |F_{obs} - kF_{calc}| / \Sigma_{hkl} F_{obs}$, where k is a scale factor and R_{free} is the R factor for the test set of reflections not used during refinement (5% of the data set).

NAD^+ synthetase (Rizzi et al., 1998), ThiI (Waterman et al., 2006), ATP sulfurylase (Mougous et al., 2006), GMP synthetase (Tesmer et al., 1996), and argininosuccinate synthetase (Goto et al., 2002, 2003; Lemke and Howell, 2001, 2002). Especially, residues 27–185, including the PP-motif (^{32}SGGVDS^{37}) (Figure 3), share high sequence similarities and form a similar overall three-dimensional structure with those of other N-type ATP pyrophosphatases, whereas residues 186–217 are unique to TilS and are designated as the TSD (TilS-specific subdomain), which consists of three helices (η1, α9, and α10) (Figure 3).

A structural comparison of the NTDs between the ATP-bound and substrate-free (1WY5) forms of TilS (Nakanishi et al., 2005) shows that residues 1–189 superposed well, with an average root mean square deviation of 0.7 Å over 189 C_α atoms, while the conformations of the residues 190–202 in the TSD are quite different (Figure 4A), including Asp191, Thr193, and Asn194 around the 3_{10} helix η1 (Figure 3). The 3_{10} helix η1 of the substrate-free form is closer to the active site by 7 Å, as compared to the ATP-bound form (Figure 4B). The distance between the α phosphate of ATP and the methyl group of Thr193 in the ATP-bound form is 5.8 Å, whereas when superposed, the methyl group of Thr193 in the substrate-free form is within 2.5 Å of the α phosphate of ATP, which disturbs ATP incorporation (Figure 4B). The NTDs of the *E. coli* (1NI5) and the ATP-bound *A. aeolicus* TilSs share 62 identical residues (39% identity), including those involved in ATP binding (Figure 3), and superposed on each other with an average root mean square deviation of 2.1 Å over 158 corresponding C_α atoms. The TSD conformation of the *E. coli* TilS was almost the same as that of the ATP-bound *A. aeolicus* TilS.

The CTD1 of the *A. aeolicus* TilS is composed of a two-layered α/β sheet (Figure 4C) and shares weak homology with Foxp2 (PDB code: 2A07), which binds specifically to DNA, according to the DALI server. The surface electrostatic distribution (Figure 4D) revealed that the CTD1 is basic and seems to be suitable for tRNA binding. The central β sheet consists of the former two β strands (β7, β8) and the latter three β strands (β9–β11) (Figure 4C). The two halves of the β sheet are connected by four hydrogen bonds between the main-chain atoms of the β8 and β11 strands, as well as by a disulfide bond between Cys253 and Cys312 (Figure 4C). The distance between the two Sγ atoms is 2.06 Å, consistent with the disulfide bond lengths of other *A. aeolicus* proteins (PDB codes: 1M1G, 1M1H, 1NPP, 1Q77, 1XM7, 2AYT, and 2DI4) (Knowlton et al., 2003; Pedone et al., 2006; Steiner et al., 2002; Suno et al., 2006), which range between 2.02 and 2.12 Å. We measured the melting temperatures of the *A. aeolicus* TilS wild-type as well as its C312A and C312S mutants by using differential scanning calorimetry (DSC), in 10 mM Tris-HCl buffer (pH 7.0) containing 300 mM NaCl. The midpoints of the melting temperatures of the wild-type and the C312A and C312S mutants are 114.2°C, 96.3°C, and 96.0°C, respectively (Figure 5). Both mutations decreased the melting temperature by 18°C.

The Active-Site Architecture

The active site is formed in the NTD of each subunit and is surrounded by the β sheet (β1–β6), and helices α5, α6, and α7 (Figure 6A). The PP-motif (^{32}SGGVDS^{37}) participates in active-site formation, whereas the second conserved motif (^{168}PLYYVKR^{174}) is located a bit farther from the active site (Figure 6A). The side chain of Arg174 is 8 Å away from the triphosphate group and is fixed by a salt bridge with Glu140, and thus it contributes to structural stabilization in the present conformation.

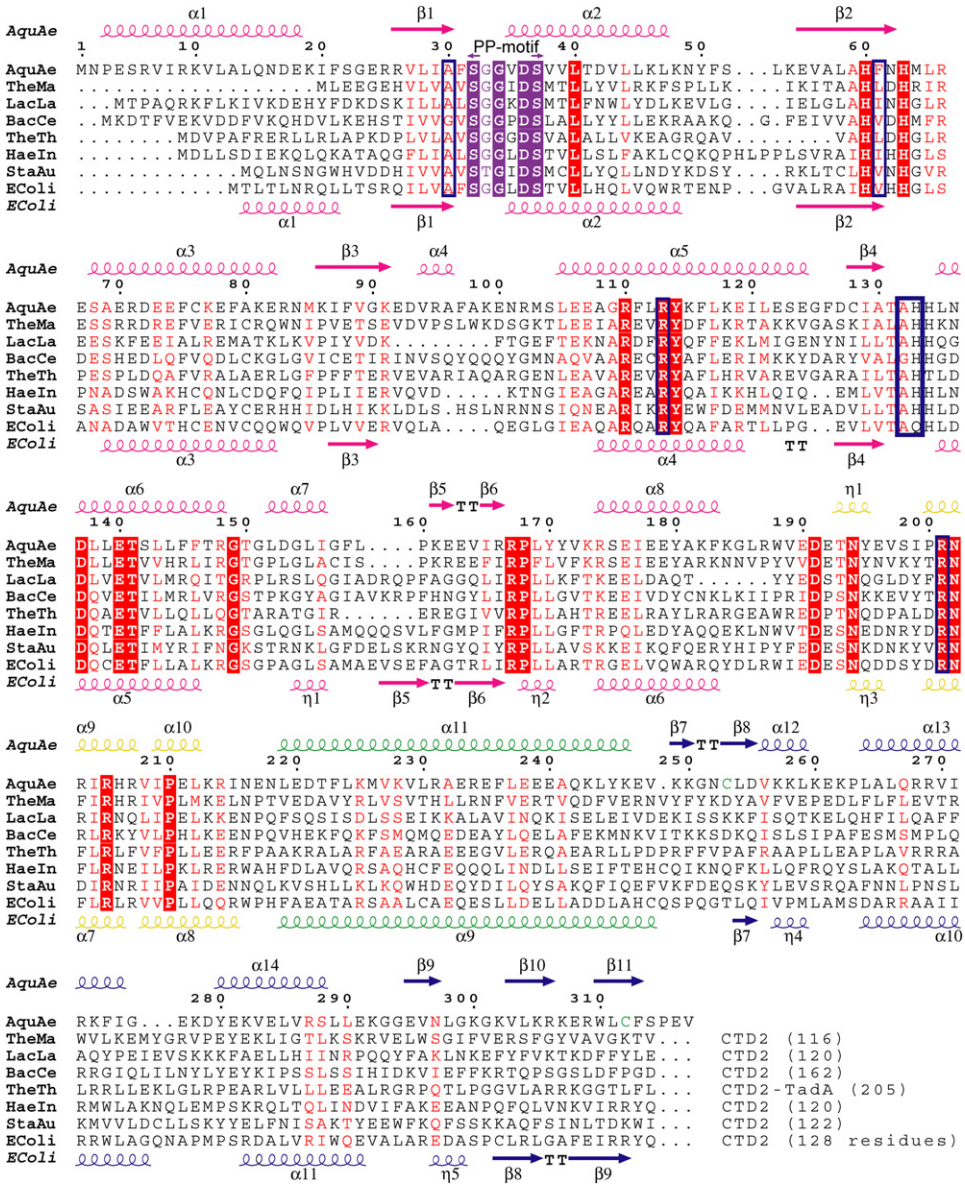

Figure 3. Sequence Alignments of TilS

The TilS sequences were aligned with ClustalX (Thompson et al., 1997), and the figure was generated with ESPript (Gouet et al., 1999, 2003). Abbreviations: AquAe, *Aquifex aeolicus*; TheMa, *Thermotoga maritima*; LacLa, *Lactococcus lactis*; BacCe, *Bacillus cereus*; TheTh, *Thermus thermophilus* HB27; HaeIn, *Haemophilus influenzae*; StaAu, *Staphylococcus aureus*; EColi, *Escherichia coli.* The secondary structures of TilS from the *A. aeolicus* and the *E. coli* are shown at the top and the bottom, respectively. The α helices and β sheets are colored according to the domain classification in Figure 2E (NTD, pink; TSD, yellow; Linker, green; and CTD1, blue). The PP-motif and the other conserved residues are white within purple- and red-filled rectangles, respectively. The highly conserved residues are colored red. The residues involved in ATP binding are enclosed in blue boxes. Cysteine residues within a disulfide bond are colored green.

The presence of the TSD causes the TilS active site to have two separate gateways: a large hole and a narrow tunnel. The large hole accommodates the ATP molecule. The adenosine moiety is buried deeply within the active site (Figures 6B and 6C), whereas the β and γ phosphate groups are located at the entrance of the hole. The size of this hole is 10 Å wide and 20 Å long, which is sufficiently large for the cytidine residue, and its periphery is positively charged (Figure 6C), which seems to be favorable to attract the negatively charged tRNA.

The shape of the second gateway into the active site is like a tunnel (Figure 6D). The L-lysine molecule is located at the entrance of the tunnel, and the distance between the α phosphate of ATP and the N_ζ atom of L-lysine is over 11 Å (Figures 4B and 6D). The L-lysine is bound weakly to the Val35, Trp188, and Asp191 side chains by

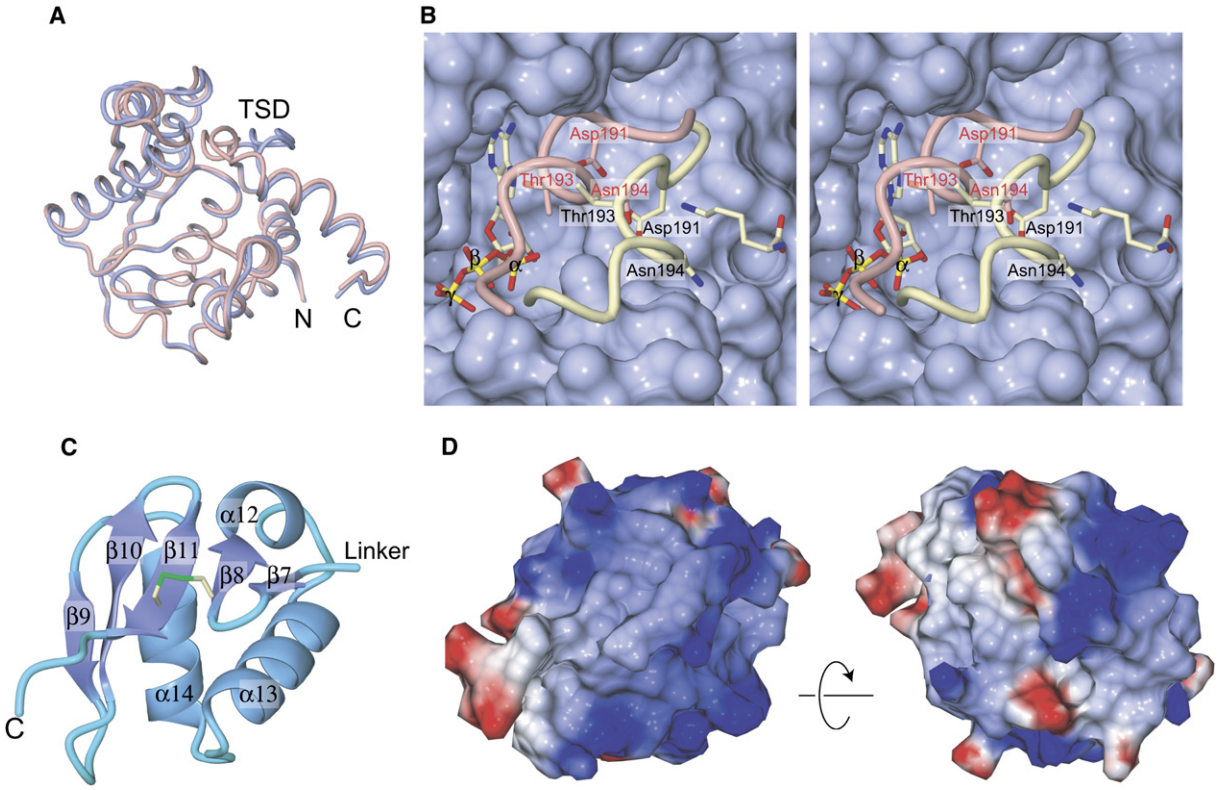

Figure 4. N- and C-Terminal Domains

The NTD superposition of the ATP-bound and the ATP-free forms of TilS, colored cyan and pink, respectively. The overall view is shown in (A), and the TSD moiety is highlighted in (B). (B) Residues 189–199 are shown in a tube model and are colored yellow (ATP-bound) and pink (ATP-free). The surface of the ATP-bound TilS without TSD is colored cyan. ATP, L-lysine, and the conserved residues are shown by stick models. (C) Ribbon representation of the CTD1. The disulfide bond is shown as a green stick model. (D) The surface of the CTD1, color coded according to the electrostatic potential (red, −10 kT/e; blue, +10 kT/e). The figure on the left is depicted in the same direction as (C), and that on the right is viewed from the opposite, as indicated by the arrow.

hydrophobic interactions, which is consistent with the report that the W188A mutant binds L-lysine weakly (Nakanishi et al., 2005). In the *A. aeolicus* TilS, Val35 in the PP-motif should be important for structural maintenance of the gateway for L-lysine. The acidic electrostatic distribution on the wall of this tunnel (Figure 6E), is achieved with several conserved residues, including Asp137, Glu140, and Asp191 (Figure 3). Asp191 is essential for the catalysis (Nakanishi et al., 2005) and would participate in the L-lysine incorporation and activation.

ATP Recognition

In order to form hydrogen-bonds with the N1 and N6 atoms of adenine, TilS uses the main-chain nitrogen and oxygen atoms of Phe61 (Figure 7A), in the same way as other N-type ATP pyrophosphatases (Rizzi et al., 1998; Tesmer et al., 1996). The adenine ring is stacked with the side chains of Arg113 and Ser32 (Figure 7A). The distances between the C5 and C6 atoms of adenine and the C_α and C_β atoms of Ser32 are 3.2 and 3.4 Å, respectively. The side chain of Ser32 is fixed by a hydrogen bond with Gly34. This sharp turn within the PP-motif is already formed in the ATP-free form and plays a structural role (Nakanishi et al., 2005). The two hydroxyl groups of the ribose hydrogen bond with the Ala30 O and Ala132 N atoms (Figure 7A). The α phosphate of ATP is 10 Å away from the PP-motif, and the β and γ phosphates point outward (Figure 7A). Arg113 hydrogen bonds with the β and γ phosphate groups. His133 binds to the γ phosphate directly in TilS/ATP/Mg/Lys (Figure 7A), whereas in TilS/AMPPNP, it binds to the γ phosphate via a water molecule (Figure 7B). This conformational difference might stem from the substitution of the oxygen atom, between the P_β and P_γ atoms in the ATP, by the nitrogen atom in the AMPPNP.

The H133A mutant reportedly binds ATP 2.5-fold more strongly, whereas the K_{cat} is subtly reduced by 1.2-fold, as compared to the wild-type TilS (Nakanishi et al., 2005). In the H133A mutant, the side chain of Arg201 or Arg167 could take the place of His133 (Figure 7A), and it could bind directly to the γ phosphate. This possible interaction would enhance the affinity for ATP but would not greatly affect the enzymatic efficiency.

Mg^{2+} Binding

In the structure of TilS/ATP/Mg/Lys, a strong spherical density was observed between the side chains of the

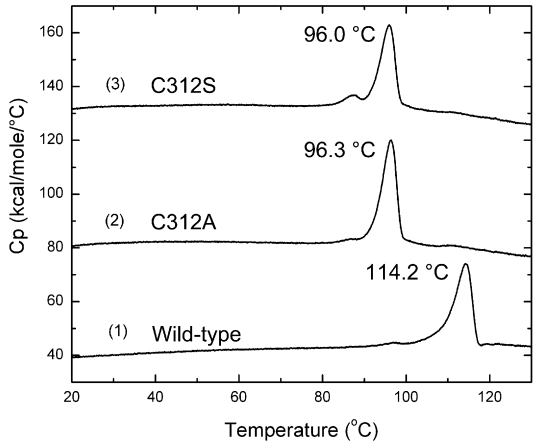

Figure 5. DSC Measurements of the *A. aeolicus* TilS Wild-Type and Its Mutants

Typical excess heat capacity curves of the *A. aeolicus* TilS at a scan rate of 90°C/hr. Curves 1, 2, and 3 represents those of the wild-type and the C312A and C312S mutants, with their peak temperatures of 114.2°C, 96.3°C, and 96.0°C, respectively.

Asp36 and Asp137 residues (Figure 2B). We considered it to be a divalent metallo-cation since it is strong and is located between two negatively charged aspartic acid residues. Mg^{2+} was the only divalent cation present during the crystallization, and thus we assigned one Mg^{2+} to this electron density. The Mg^{2+} is mainly coordinated by the carboxyl side chains of the conserved Asp36 (2.6 Å) and Asp137 (2.8 Å) residues (Figure 2B), which explains why the D36A and D137A mutants lack enzymatic activity (Nakanishi et al., 2005). In addition, the Ala132 O atom (3.4 Å), the hydroxyl group of the ribose (3.0 Å), and a water molecule associated with His134 (2.6 Å) (Figure 7A) participate in the Mg^{2+} coordination. The coordination of Mg^{2+} by five ligands in proteins is less common than six coordination, but the octahedral distribution of the five oxygen atoms (Figure 7A) satisfies the geometry of the Mg^{2+}-ligand interaction in proteins (Harding, 2001). We consider that the Mg^{2+} binding by the negatively charged carboxyl groups of two aspartic acid residues would be stronger, as compared to the other ligands, and thus would compensate for the lack of the sixth ligand. There are no significant differences between the active site structures with and without the Mg^{2+}, indicating that the role of the Mg^{2+} is not structural.

The role of the Mg^{2+} during ATP hydrolysis was investigated extensively in aminoacyl-tRNA synthetase (aaRS), which attaches amino acids to tRNA by using ATP (Ibba et al., 2005). The Mg^{2+} usually bridges the β and γ phosphate moieties of the ATP, so that the β phosphate group is fixed. This conformation is suitable for the nucleophilic attack on the α phosphate, and the Mg^{2+} facilitates the release of the pyrophosphate group. The Mg^{2+} also contributes to the withdrawal of electrons from the phosphate groups, which assists in the hydrolysis of the phosphodiester bond of ATP. Thus, the Mg^{2+} located in the active site of TilS is considered to be involved in the formation of the adenylated cytidine. The Mg^{2+} coordination by the conserved aspartic acid residue in the signature PP-motif would be common among the N-type ATP pyrophosphatases.

DISCUSSION

We identified the TilS residues that interact with the ATP and found that the triphosphate moiety is located opposite the PP-motif (Figure 7A). Among the N-type ATP pyrophosphatases, the structure of GMP synthetase (1GPM), containing AMP, Mg^{2+}, and pyrophosphate, represents the state after ATP hydrolysis (Figure 7C) (Tesmer et al., 1996). A structural comparison suggested that a conformational change of the phosphate moieties of ATP occurs during the formation of the adenylated intermediate, but the positions of the Mg^{2+} ions do not differ greatly (Figures 7A and 7C). The Mg^{2+}, coordinated by Asp36 in the structure of TilS, seems to be ready to interact with the phosphate moieties of the ATP. When the Mg^{2+} interacts with ATP, the Asp36 side chain would rotate outside, as observed in GMP synthetase (Figure 7C). More information about the ATP conformational change is available from the structures of *E. coli* argininosuccinate synthetase, another N-type ATP pyrophosphatase. The present conformation of ATP in TilS is similar to the extended conformation observed in *E. coli* argininosuccinate synthetase (1KP2) (Lemke and Howell, 2002), which binds to ATP, citrulline, and L-aspartate, to synthesize argininosuccinate. The β and γ phosphate moieties of the ATP occupy the aspartate binding site in the extended conformation (Figure 7D). When the aspartate binding site is occupied (1KP3) (Lemke and Howell, 2002), the β and γ phosphates of the ATP adopt a U-shaped conformation and associate with the PP-motif (Figure 7E). Similarly, we expect that the binding of $tRNA^{Ile}_2$ to TilS would flip the β and γ phosphates of the ATP. This conformational change of the ATP in *A. aeolicus* TilS appears to be more difficult to achieve, as compared to that in the *E. coli* argininosuccinate synthetase, because the hydrogen bonds with Arg113 tightly hold the ATP (Figure 7A). However, the negatively charged tRNA should repel the ATP strongly enough to induce its conformational change.

The role of the Mg^{2+} in TilS, as well as its mechanistic implications, is discussed further based on a structural comparison with that of lysyl-tRNA synthetase (LysU), which catalyzes a similar reaction to TilS, in that it attaches L-lysine to tRNA by using ATP. The ATP in LysU adopts the U-shaped conformation, and the adenylation occurs by an inline displacement mechanism (Desogus et al., 2000). The position of the Mg^{2+} in TilS was compared to those of the three Mn^{2+}, an analog of Mg^{2+}, which associate with the U-shaped ATP in LysU (Desogus et al., 2000), by superposition based on the adenosine moieties of ATP (Figure 7F). The present position of the Mg^{2+} in TilS is near the Mn1 in LysU, suggesting that the Mg^{2+} would interact with the phosphates of the ATP. In this context, one Mn^{2+} ion that interacts with the β and γ phosphates in LysU is widely shared among the class 1 and class 2 aaRSs, and the other two Mn^{2+} ions are unique to the class 2 aaRSs (Ibba et al., 2005). Therefore, it is possible that two (or more) Mg^{2+} ions

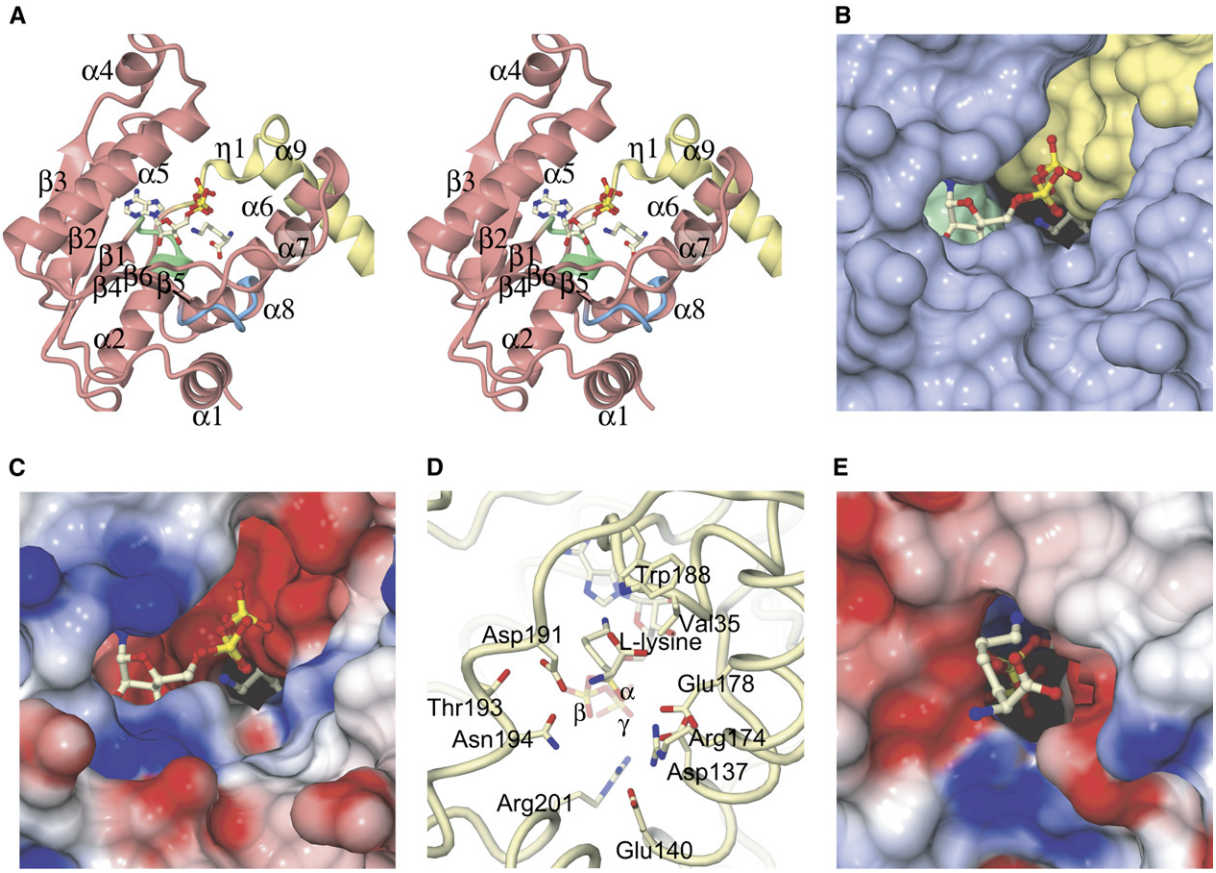

Figure 6. The Active-Site Architecture

(A) A stereoview of the active site. The ATP and L-lysine molecules are shown by stick models. The PP-motif (^{32}SGGVDS^{37}), the second conserved motif (^{168}PLYYVKR^{174}), and the TilS-specific subdomain (TSD) are colored green, blue, and yellow, respectively. The other parts are colored pink.

(B and C) Surface models of the active site, viewed from the large hole. The surface of the protein moiety was calculated. The ligands are shown by stick models. The PP-motif and the TSD are colored green and yellow, respectively in (B) and are color coded according to the electrostatic potential in (C) (red, −10 kT/e; blue, +10 kT/e).

(D) The residues that constitute the wall of the narrow tunnel are shown in stick models.

(E) The surface of the narrow tunnel, depicted in the same direction as (D) and color coded according to the electrostatic potential (red, −10 kT/e; blue, +10 kT/e).

are present within the active site of TilS in the transition state and interact not only with the β and γ phosphates, but also with the α and β phosphates. In the active site of TilS, the pocket into which the pyrophosphate group sits after the conformational change is negatively charged (Figures 6B and 6C). Thus, Mg^{2+} binding in the active site of TilS counteracts the acidity, to reduce the destabilizing effect of the electrostatic repulsion between TilS and the pyrophosphate moiety of the ATP.

The docking model of TilS with AMP, $tRNA^{Ile}_2$, and L-lysine was reported previously (Nakanishi et al., 2005). Based on considerations of the conformational change of the pyrophosphate moiety of ATP, we revised the model. In our docking model of TilS with $tRNA^{Ile}_2$ (Figure 7G), the cytidine residue satisfies the inline displacement mechanism for the attack on the α phosphate, and the phosphate of the tRNA backbone takes the place formerly occupied by the γ phosphate of ATP in the extended conformation, which would drive the ATP to flip. If the ATP flips freely so that the phosphate moieties can approach the Mg^{2+}, then the Mg^{2+} can facilitate the water-mediated cleavage of the phosphodiester bond in the absence of $tRNA^{Ile}_2$. Thus, keeping the triphosphate moieties of the ATP away from the Mg^{2+} in the absence of $tRNA^{Ile}_2$ should be beneficial for preventing wasteful ATP hydrolysis. Taken together, the present ATP conformation (Figure 7A) represents the initial binding state, and the triphosphate moiety would flip upon the incorporation of the cytidine residue of $tRNA^{Ile}_2$ inside the active site.

In order to complete the second reaction, the adenylated cytidine and L-lysine come close to each other. Since the two hydrogen bonds with Phe61 and the stacking interactions by Ser32 and Arg113 fix the adenine ring, a large translocation of the adenosine moiety would be unlikely to occur. Therefore, we expect that the L-lysine would be carried over a long distance for lysidine formation (Figure 7G). We observed different conformations of the TSD between the ATP-bound and -free forms (Figures

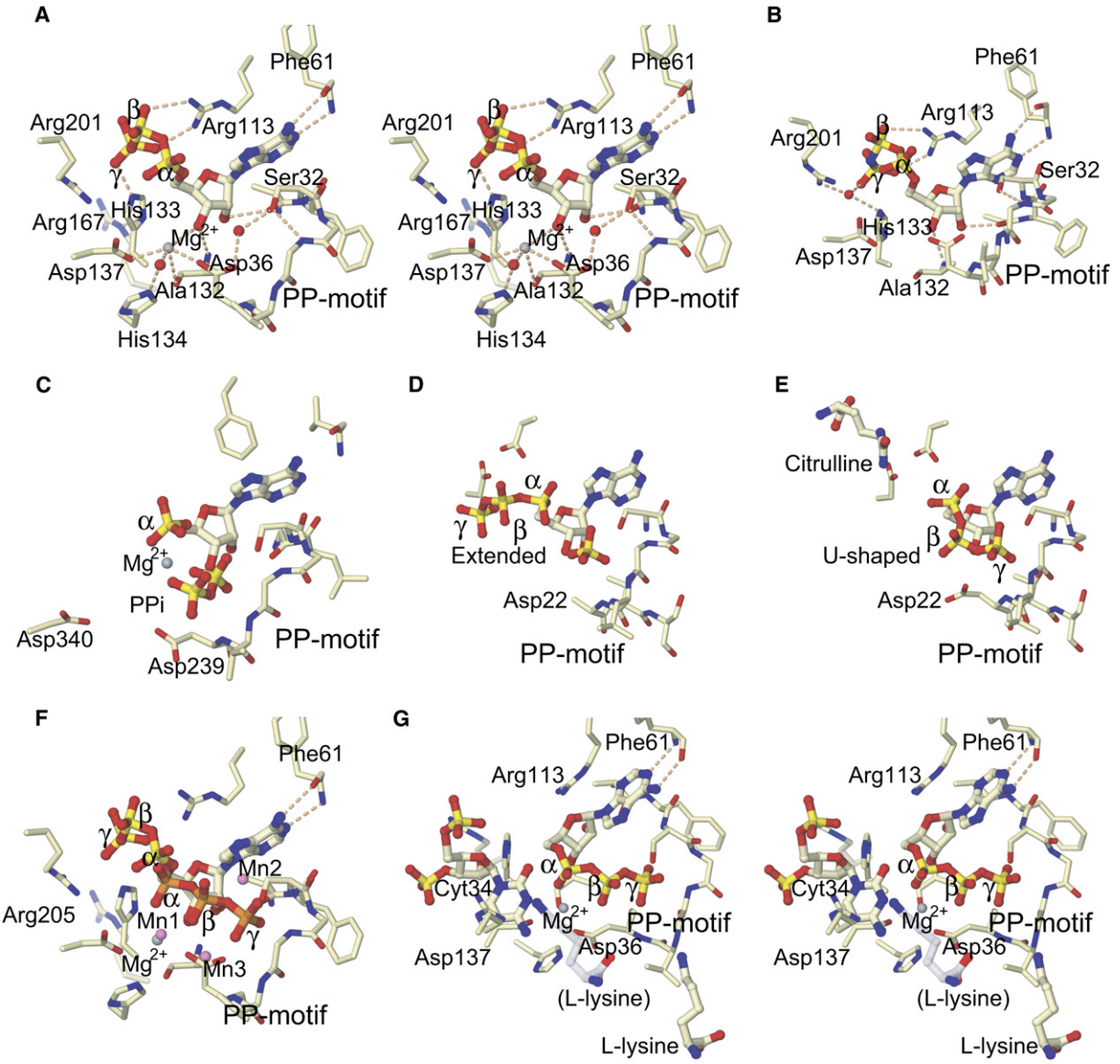

Figure 7. ATP Recognition

(A) The amino acid residues that recognize the ATP and Mg^{2+} (stereoview). The ATP is shown by a stick model. The Mg^{2+} and water molecules are shown as gray and red spheres, respectively. Hydrogen bonds are shown as dotted lines.

(B) Recognition of the AMPPNP, shown as in (A). The nitrogen atom between the P_β and P_γ atoms is colored blue.

(C) AMP and pyrophosphate binding by *E. coli* GMP synthetase, depicted as in (A).

(D and E) Extended (D) and U-shaped (E) ATP conformations in the structures of the *E. coli* argininosuccinate synthetase complexed with ATP (D) and with both ATP and citrulline (E), respectively. The side chain of Asp22 in (D) is missing in the coordinates (1KP2).

(F) Comparison of the ATP conformation. The U-shaped ATP, with three manganese ions (Mn1, Mn2, and Mn3) in the structure of LysU (PDB code: 1E24) was superposed based on the adenine ring. The phosphate atoms are colored orange, and the manganese ions are colored magenta.

(G) Docking model of TilS and the cytidine residue of $tRNA^{Ile}_2$ (stereoview). The phosphate atoms of the ATP and the side chain of Asp36 were moved manually. The L-lysine was moved manually, and the model structure is colored light gray and is indicated as (L-lysine).

4A and 4B), indicating that the TSD could be mobile during lysidine synthesis. The D191A and N194A mutants reportedly lack enzymatic activity (Nakanishi et al., 2005), and these residues are located where they could interact with the L-lysine (Figure 4B). The movement of the TSD would carry the L-lysine into the active site, which could be triggered by the $tRNA^{Ile}_2$ binding. The structure of TilS complexed with $tRNA^{Ile}_2$ will reveal the precise conformational changes that occur during lysidine synthesis and confirm the catalytic mechanism.

We have shown that a disulfide bond stabilizes the structure of *A. aeolicus* TilS, which is considered to be an adaptation to the thermophilic environment. TilS without the disulfide bond (C312A and C312S mutants) starts

to denature near 95°C, the maximal growth temperature of *A. aeolicus* (Deckert et al., 1998), whereas the wild-type protein is stable at 95°C (Figure 5). Even though the melting temperatures in vivo would not exactly agree with those in vitro, due to the different concentrations of salt and other compounds, the gap would be no more than a couple of degrees, since the addition of 4 mM AMPPNP increased them only by 1.1°C–1.6°C (data not shown). Thus, the disulfide bond formation is considered to be vital for the stabilization of the *A. aeolicus* TilS in vivo. We analyzed the TilS sequences from other thermophilic bacteria to determine whether they could form disulfide bonds. The TilS sequences from *Thermotoga maritima* and *Thermus thermophilus* have two and four cysteine residues, respectively. Cys61 and Cys137 in the *T. maritima* TilS correspond to Ala80 and Gly157 in the *A. aeolicus* TilS (Figure 3), which are over 20 Å apart from each other, indicating that the *T. maritima* TilS has no disulfide bond. On the other hand, the four cysteine residues in the *T. thermophilus* TilS are clustered in the TadA domain, which is fused to the C terminus of TilS. TadA generates inosine on $tRNA^{Arg}_2$ (Wolf et al., 2002), and the two cysteine residues are required for the coordination of a zinc ion (Kuratani et al., 2005). This TilS-TadA fusion protein might be stabilized, as compared to when the proteins exist separately, or it may catalyze the tRNA modification reactions efficiently, which might represent another adaptation by *T. thermophilus* to the thermophilic environment.

Another example is the tRNA adenosine N1 methyltransferase from *Pyrococcus abyssi*, which is a tetrameric enzyme containing four intersubunit disulfide bonds, while its homologs from *T. thermophilus* and *Saccharomyces cerevisiae* lack disulfide bonds (Roovers et al., 2004). Systematic structural studies will establish the notion that structural disulfide bonds are prevalent in certain thermophilic organisms.

EXPERIMENTAL PROCEDURES

Purification of the *A. aeolicus* TilS

The *A. aeolicus* TilS gene was cloned into the pET15b vector (Novagen) at the NcoI and BamHI sites, and the recombinant protein was expressed in *E. coli* strain BL21 (DE3) codonplus RIL (Stratagene) by induction with 1 mM IPTG overnight at 37°C. The *E. coli* cells were sonicated in 20 mM Tris-HCl buffer (pH 8.5) containing 500 mM NaCl, 5 mM $MgCl_2$, and 10 mM 2-mercaptoethanol, and the lysate was centrifuged at 30,000 × g for 10 min. The protein solution was heated at 80°C for 20 min to denature the *E. coli* proteins. After the centrifugation, an ammonium sulfate solution was added to the supernatant to a final concentration of 1.1 M, and then the protein solution was applied to a Butyl Toyopearl column (Tosoh), which was eluted by linearly decreasing the ammonium sulfate concentration. The protein was collected and dialyzed against 20 mM Tris-HCl buffer (pH 7.0) containing 50 mM NaCl and 10 mM 2-mercaptoethanol. It was applied to a Resource S (Amersham Biosciences) column by using the AKTA system and was eluted by a linear gradient of NaCl from 50 mM to 1 M in 20 mM Tris-HCl buffer (pH 7.0) containing 10 mM 2-mercaptoethanol. The purified protein was concentrated to 7 mg/ml in 10 mM Tris-HCl buffer (pH 7.0) containing 300 mM NaCl. The plasmids encoding the C312A and C312S mutants were prepared by PCR. The mutant proteins were expressed and purified in the same way as the wild-type, and were concentrated to 0.8 mg/ml in 10 mM Tris-HCl buffer (pH 7.0) containing 300 mM NaCl.

The gene encoding *A. aeolicus* $tRNA^{Ile2}$ was PCR-amplified and cloned into the pUC19 plasmid (Takara). *A. aeolicus* $tRNA^{Ile2}$ was transcribed in vitro with T7 RNA polymerase and purified in the same condition as described for *P. horikoshii* $tRNA^{Val}$ (Ishitani et al., 2003).

Crystallization, Data Collection, Structure Determination, and Refinement

The crystallization was performed by the hanging vapor diffusion method at 20°C. At first, crystallization was performed with a protein-tRNA solution containing 7 mg/ml TilS with a 1:1.1 molar ratio of TilS:$tRNA^{Ile}_2$ in 50 mM HEPES-Na buffer (pH 7.6), containing 300 mM NaCl, 5 mM $MgCl_2$, 1 mM DTT, 2 mM AMPPNP, and 2 mM L-lysine. We used AMPPNP, an analog of ATP, expecting that AMPPNP would not react with tRNA at 20°C, in order to capture the state just before the reaction. Crystals were grown in a drop composed of 1 μl solution and an equal volume of the reservoir solution (0.1 M citrate-Na buffer [pH 5.8] containing 0.2 M ammonium acetate and 20% PEG 4,000). The crystal was transferred into reservoir solution containing 15% glycerol, and the diffraction data set was collected on beamline BL41XU at the SPring8 (Japan). The data were processed with the program HKL2000 (Otwinowski and Minor, 1997). As described below, this crystal contained AMPPNP but neither tRNA nor L-lysine. Therefore, we refer to this sample as TilS/AMPPNP. The TilS/AMPPNP crystal belongs to the space group $P2_1$, with unit cell parameters of a = 94.5 Å, b = 82.2 Å, c = 109.4 Å, and β = 105.9°.

We determined the structure of TilS/AMPPNP by molecular replacement with the program MOLREP (Vagin and Teplyakov, 1997) by using the coordinates of the substrate-free form of *A. aeolicus* TilS (1WY5) comprising residues 1–311. Four molecules (A–D) were found in the asymmetric unit. At first, 20 residues in the C-terminal domain (291–311) did not fit the electron density well. We changed these into alanine residues, drew the electron density map, and manually assigned the side chains. The model building was done with O (Jones et al., 1991) and CueMol (http://cuemol.sourceforge.jp/en/). In the final model, molecule A contained all residues (1–317), and molecules B–D contained residues 1–314. Each of the four molecules contained a disulfide bond between Cys253 and Cys312. The electron densities corresponding to AMPPNP were observed in two molecules (A and C) out of the four in the asymmetric unit. No electron densities for either L-lysine or tRNA were detected. The TilS/AMPPNP model was refined up to 2.7 Å resolution by using the program CNS (Adams et al., 1997), with final R_{free} and R_{work} factors of 29.4% and 22.6%, respectively (Table 1).

During this study, the K_m values for ATP and L-lysine, determined by the steady state kinetics of *A. aeolicus* TilS, were reported to be 19.4 and 629.4 μM, respectively (Nakanishi et al., 2005). According to the K_m value of ATP, all of the active sites should be occupied by 2 mM AMPPNP. However, the reagents in the crystallization might reduce the binding affinity of TilS for the substrates, due to the possible change in the dielectric constant of the solution. The affinity for L-lysine is lower than that for ATP by about 30-fold, and thus we consider this to be the reason for its absence from the crystal of TilS/AMPPNP.

In order to obtain the crystal of TilS containing four ATPs in all four molecules in the asymmetric unit, as well as L-lysine, we increased their concentrations to 4 mM (ATP) and 50 mM (L-lysine). We used ATP instead of AMPPNP, since the hydrolysis of ATP would not occur in the absence of tRNA. As described below, this crystal contained ATP, Mg^{2+}, and L-lysine, and therefore we refer to it as TilS/ATP/Mg/Lys. The crystals of TilS/ATP/Mg/Lys were grown in a drop composed of 1 μl protein solution (7 mg/ml TilS in 10 mM Tris-HCl buffer [pH 7.0] containing 300 mM NaCl, 10 mM $MgCl_2$, 1 mM 2-mercaptoethanol, 4 mM ATP, and 50 mM L-lysine) and an equal volume of the reservoir solution (0.1 M citrate-Na buffer [pH 5.4], containing 0.2 M ammonium acetate and 20% PEG 4,000). The crystals grew in 2 weeks. The Mg^{2+} concentration was increased twice so that its proportion to the ATP remained the same, as compared to the conditions for TilS/AMPPNP. Increasing the concentration of L-lysine above 50 mM did not yield any crystals under the conditions we searched. When the crystal grown in

the presence of 50 mM L-lysine was soaked in a higher concentration of L-lysine, it started to melt.

The TilS/ATP/Mg/Lys crystal was transferred into 0.1 M citrate buffer (pH 5.4) containing 0.2 M ammonium acetate, 20% PEG 4,000, 15% glycerol, 4 mM ATP, 10 mM $MgCl_2$, and 50 mM L-lysine, and the diffraction data set was collected on beamline BL41XU at the SPring8 (Japan). The data were processed with the program HKL2000 (Otwinowski and Minor, 1997). The crystal of TilS/ATP/Mg/Lys belongs to the space group $P2_1$, with unit cell parameters of a = 97.4 Å, b = 81.6 Å, c = 109.1 Å, and $\beta = 106.0^\circ$. The change in the cell constant of a from 94.5 Å to 97.4 Å (changed by 3%) suggests that the crystal of TilS/ATP/Mg/Lys is nonisomorphous to that of TilS/AMPPNP, which would be caused by the increased concentrations of L-lysine and ATP in the crystal. A strong spherical density was observed between the side chains of the Asp36 and Asp137 residues in molecule C. Associations with two negatively charged aspartic acid residues suggest that it would be a divalent cation. Since the crystallization conditions contained Mg^{2+} as the only divalent cation, we assigned the Mg^{2+} to this strong electron density. We could not find any significant structural differences between the active sites with and without the Mg^{2+}.

The TilS/ATP/Mg/Lys structure was determined by molecular replacement with the program MOLREP (Vagin and Teplyakov, 1997) and was refined up to 2.5 Å resolution by using the program CNS (Adams et al., 1997), with final R_{free} and R_{work} factors of 27.4% and 22.9%, respectively (Table 1). In the final model, molecule A contains all residues (1–317), molecules B and C contain residues 1–314, and molecule D contains residues 1–313. All four molecules contain the ATP, molecule B contains the L-lysine, and molecule C contains the Mg^{2+}. The terminal amino and carboxyl atoms of the L-lysine interact with Arg203 of molecule C, and Glu211 and Arg214 of molecule D, which is considered to be due to the crystal packing. The Ramachandran plot analyses with PROCHECK (Laskowski et al., 1993) revealed that both models showed good stereochemistry (Table 1).

Differential Scanning Calorimetry

Differential scanning calorimetry (DSC) was carried out with a VP-capillary DSC platform (MicroCal, USA) up to 130°C, at scan rates of 90°C/hr, to determine the unfolding transition temperatures of the *A. aeolicus* TilS wild-type and the C312A and C312S mutants. The proteins were concentrated to 0.8 mg/ml in 10 mM Tris-HCl buffer (pH 7.0) containing 300 mM NaCl, filtered through a 0.22 μm pore size membrane, and degassed before measurements.

ACKNOWLEDGMENTS

We are grateful to M. Kawamoto and N. Shimizu for technical assistance in the data collection at BL41XU at SPring-8. We thank S. Sekine for help with the data processing for TilS/AMPPNP and fruitful advice on the catalytic mechanism of aaRS. We are grateful to the reviewers for insightful comments. We thank M. Sawano, T. Yanagisawa, and M. Takehira for help with the DSC measurements. We thank T. Nakayama, K. Yajima, and A. Ishii for clerical help. This work was supported by the RIKEN Structural Genomics/Proteomics Initiative (RSGI), the National Project on Protein Structural and Functional Analyses, Ministry of Education, Culture, Sports, Science and Technology of Japan, and by the Fellowship for Young Scientists from the JSPS (Japan Society for the Promotion of Science) to M.K.

Received: May 20, 2007
Revised: September 6, 2007
Accepted: September 25, 2007
Published: December 11, 2007

REFERENCES

Adams, P.D., Pannu, N.S., Read, R.J., and Brunger, A.T. (1997). Cross-validated maximum likelihood enhances crystallographic simulated annealing refinement. Proc. Natl. Acad. Sci. USA *94*, 5018–5023.

Agris, P.F., Vendeix, F.A., and Graham, W.D. (2007). tRNA's wobble decoding of the genome: 40 years of modification. J. Mol. Biol. *366*, 1–13.

Beeby, M., O'Connor, B.D., Ryttersgaard, C., Boutz, D.R., Perry, L.J., and Yeates, T.O. (2005). The genomics of disulfide bonding and protein stabilization in thermophiles. PLoS Biol. *3*, e309.

Bjork, G., and Hagervall, T.G. (2005). Transfer RNA modification. In Escherichia coli and Salmonella: Cellular and Molecular Biology, R. Curtiss, III, A. Bock, J.L. Ingrahan, J.B. Kaper, S. Maloy, F.C. Neidhardt, M.M. Riley, C.L. Squires, and B.L. Wanner, eds. (Washington, DC: ASM Press) (http://www.ecosal.org/).

Bork, P., and Koonin, E.V. (1994). A P-loop-like motif in a widespread ATP pyrophosphatase domain: implications for the evolution of sequence motifs and enzyme activity. Proteins *20*, 347–355.

Crick, F.H. (1966). Codon-anticodon pairing: the wobble hypothesis. J. Mol. Biol. *19*, 548–555.

Deckert, G., Warren, P.V., Gaasterland, T., Young, W.G., Lenox, A.L., Graham, D.E., Overbeek, R., Snead, M.A., Keller, M., Aujay, M., et al. (1998). The complete genome of the hyperthermophilic bacterium *Aquifex aeolicus*. Nature *392*, 353–358.

DeDecker, B.S., O'Brien, R., Fleming, P.J., Geiger, J.H., Jackson, S.P., and Sigler, P.B. (1996). The crystal structure of a hyperthermophilic archaeal TATA-box binding protein. J. Mol. Biol. *264*, 1072–1084.

Desogus, G., Todone, F., Brick, P., and Onesti, S. (2000). Active site of lysyl-tRNA synthetase: structural studies of the adenylation reaction. Biochemistry *39*, 8418–8425.

Gerber, A.P., and Keller, W. (1999). An adenosine deaminase that generates inosine at the wobble position of tRNAs. Science *286*, 1146–1149.

Goto, M., Nakajima, Y., and Hirotsu, K. (2002). Crystal structure of argininosuccinate synthetase from *Thermus thermophilus* HB8. Structural basis for the catalytic action. J. Biol. Chem. *277*, 15890–15896.

Goto, M., Omi, R., Miyahara, I., Sugahara, M., and Hirotsu, K. (2003). Structures of argininosuccinate synthetase in enzyme-ATP substrates and enzyme-AMP product forms: stereochemistry of the catalytic reaction. J. Biol. Chem. *278*, 22964–22971.

Gouet, P., Courcelle, E., Stuart, D.I., and Metoz, F. (1999). ESPript: analysis of multiple sequence alignments in PostScript. Bioinformatics *15*, 305–308.

Gouet, P., Robert, X., and Courcelle, E. (2003). ESPript/ENDscript: extracting and rendering sequence and 3D information from atomic structures of proteins. Nucleic Acids Res. *31*, 3320–3323.

Harding, M.M. (2001). Geometry of metal-ligand interactions in proteins. Acta Crystallogr. D Biol. Crystallogr. *57*, 401–411.

Ibba, M., Francklyn, C., and Cusack, S. (2005). The Aminoacyl-tRNA Synthetases (Austin, TX: Landes Bioscience).

Ikeuchi, Y., Soma, A., Ote, T., Kato, J., Sekine, Y., and Suzuki, T. (2005). Molecular mechanism of lysidine synthesis that determines tRNA identity and codon recognition. Mol. Cell *19*, 235–246.

Ishitani, R., Nureki, O., Nameki, N., Okada, N., Nishimura, S., and Yokoyama, S. (2003). Alternative tertiary structure of tRNA for recognition by a posttranscriptional modification enzyme. Cell *113*, 383–394.

Jones, T.A., Zou, J.Y., Cowan, S.W., and Kjeldgaard, M. (1991). Improved methods for binding protein models in electron density maps and the location of errors in these models. Acta Crystallogr. A *47*, 110–119.

Karlstrom, M., Stokke, R., Steen, I.H., Birkeland, N.K., and Ladenstein, R. (2005). Isocitrate dehydrogenase from the hyperthermophile *Aeropyrum pernix*: X-ray structure analysis of a ternary enzyme-substrate complex and thermal stability. J. Mol. Biol. *345*, 559–577.

Knowlton, J.R., Bubunenko, M., Andrykovitch, M., Guo, W., Routzahn, K.M., Waugh, D.S., Court, D.L., and Ji, X. (2003). A spring-loaded state of NusG in its functional cycle is suggested by X-ray crystallography and supported by site-directed mutants. Biochemistry *42*, 2275–2281.

Kuratani, M., Ishii, R., Bessho, Y., Fukunaga, R., Sengoku, T., Shirouzu, M., Sekine, S., and Yokoyama, S. (2005). Crystal structure of tRNA adenosine deaminase (TadA) from *Aquifex aeolicus*. J. Biol. Chem. *280*, 16002–16008.

Laskowski, R.A., MacArthur, M.W., Moss, A.L., and Thornton, J.M. (1993). PROCHECK. J. Appl. Crystallogr. *26*, 283–291.

Lemke, C.T., and Howell, P.L. (2001). The 1.6 Å crystal structure of *E. coli* argininosuccinate synthetase suggests a conformational change during catalysis. Structure *9*, 1153–1164.

Lemke, C.T., and Howell, P.L. (2002). Substrate induced conformational changes in argininosuccinate synthetase. J. Biol. Chem. *277*, 13074–13081.

Mallick, P., Boutz, D.R., Eisenberg, D., and Yeates, T.O. (2002). Genomic evidence that the intracellular proteins of archaeal microbes contain disulfide bonds. Proc. Natl. Acad. Sci. USA *99*, 9679–9684.

Marck, C., and Grosjean, H. (2002). tRNomics: analysis of tRNA genes from 50 genomes of Eukarya, Archaea, and Bacteria reveals anticodon-sparing strategies and domain-specific features. RNA *8*, 1189–1232.

Meyer, J., Clay, M.D., Johnson, M.K., Stubna, A., Munck, E., Higgins, C., and Wittung-Stafshede, P. (2002). A hyperthermophilic plant-type [2Fe-2S] ferredoxin from *Aquifex aeolicus* is stabilized by a disulfide bond. Biochemistry *41*, 3096–3108.

Mougous, J.D., Lee, D.H., Hubbard, S.C., Schelle, M.W., Vocadlo, D.J., Berger, J.M., and Bertozzi, C.R. (2006). Molecular basis for G protein control of the prokaryotic ATP sulfurylase. Mol. Cell *21*, 109–122.

Muramatsu, T., Nishikawa, K., Nemoto, F., Kuchino, Y., Nishimura, S., Miyazawa, T., and Yokoyama, S. (1988a). Codon and amino-acid specificities of a transfer RNA are both converted by a single post-transcriptional modification. Nature *336*, 179–181.

Muramatsu, T., Yokoyama, S., Horie, N., Matsuda, A., Ueda, T., Yamaizumi, Z., Kuchino, Y., Nishimura, S., and Miyazawa, T. (1988b). A novel lysine-substituted nucleoside in the first position of the anticodon of minor isoleucine tRNA from *Escherichia coli*. J. Biol. Chem. *263*, 9261–9267.

Nakanishi, K., Fukai, S., Ikeuchi, Y., Soma, A., Sekine, Y., Suzuki, T., and Nureki, O. (2005). Structural basis for lysidine formation by ATP pyrophosphatase accompanied by a lysine-specific loop and a tRNA-recognition domain. Proc. Natl. Acad. Sci. USA *102*, 7487–7492.

Otwinowski, Z., and Minor, W. (1997). Processing of X-ray diffraction data collected in oscillation mode. Methods Enzymol. *276*, 307–326.

Pedone, E., D'Ambrosio, K., De Simone, G., Rossi, M., Pedone, C., and Bartolucci, S. (2006). Insights on a new PDI-like family: structural and functional analysis of a protein disulfide oxidoreductase from the bacterium *Aquifex aeolicus*. J. Mol. Biol. *356*, 155–164.

Rizzi, M., Bolognesi, M., and Coda, A. (1998). A novel deamido-NAD+-binding site revealed by the trapped NAD-adenylate intermediate in the NAD+ synthetase structure. Structure *6*, 1129–1140.

Roovers, M., Wouters, J., Bujnicki, J.M., Tricot, C., Stalon, V., Grosjean, H., and Droogmans, L. (2004). A primordial RNA modification enzyme: the case of tRNA (m1A) methyltransferase. Nucleic Acids Res. *32*, 465–476.

Silva, F.J., Belda, E., and Talens, S.E. (2006). Differential annotation of tRNA genes with anticodon CAT in bacterial genomes. Nucleic Acids Res. *34*, 6015–6022.

Soma, A., Ikeuchi, Y., Kanemasa, S., Kobayashi, K., Ogasawara, N., Ote, T., Kato, J., Watanabe, K., Sekine, Y., and Suzuki, T. (2003). An RNA-modifying enzyme that governs both the codon and amino acid specificities of isoleucine tRNA. Mol. Cell *12*, 689–698.

Steiner, T., Kaiser, J.T., Marinkovic, S., Huber, R., and Wahl, M.C. (2002). Crystal structures of transcription factor NusG in light of its nucleic acid- and protein-binding activities. EMBO J. *21*, 4641–4653.

Suno, R., Niwa, H., Tsuchiya, D., Zhang, X., Yoshida, M., and Morikawa, K. (2006). Structure of the whole cytosolic region of ATP-dependent protease FtsH. Mol. Cell *22*, 575–585.

Suzuki, T. (2005). Biosynthesis and function of tRNA wobble modifications. In Fine-Tuning of RNA Functions by Modification and Editing, H. Grosjean, ed. (Heidelberg: Springer), pp. 23–60.

Tesmer, J.J., Klem, T.J., Deras, M.L., Davisson, V.J., and Smith, J.L. (1996). The crystal structure of GMP synthetase reveals a novel catalytic triad and is a structural paradigm for two enzyme families. Nat. Struct. Biol. *3*, 74–86.

Thompson, J.D., Gibson, T.J., Plewniak, F., Jeanmougin, F., and Higgins, D.G. (1997). The CLUSTAL_X windows interface: flexible strategies for multiple sequence alignment aided by quality analysis tools. Nucleic Acids Res. *25*, 4876–4882.

Toth, E.A., Worby, C., Dixon, J.E., Goedken, E.R., Marqusee, S., and Yeates, T.O. (2000). The crystal structure of adenylosuccinate lyase from *Pyrobaculum aerophilum* reveals an intracellular protein with three disulfide bonds. J. Mol. Biol. *301*, 433–450.

Vagin, A., and Teplyakov, A. (1997). MOLREP: an automated program for molecular replacement. J. Appl. Crystallogr. *30*, 1022–1025.

Vieille, C., and Zeikus, G.J. (2001). Hyperthermophilic enzymes: sources, uses, and molecular mechanisms for thermostability. Microbiol. Mol. Biol. Rev. *65*, 1–43.

Waterman, D.G., Ortiz-Lombardia, M., Fogg, M.J., Koonin, E.V., and Antson, A.A. (2006). Crystal structure of *Bacillus anthracis* ThiI, a tRNA-modifying enzyme containing the predicted RNA-binding THUMP domain. J. Mol. Biol. *356*, 97–110.

Wolf, J., Gerber, A.P., and Keller, W. (2002). tadA, an essential tRNA-specific adenosine deaminase from *Escherichia coli*. EMBO J. *21*, 3841–3851.

Yokoyama, S., and Nishimura, S. (1995). Modified nucleosides and codon recognition. In tRNA: Structure, Biosynthesis, and Function, D. Soll and U. RajBhandary, eds. (Washington, DC: ASM Press), pp. 207–224.

Accession Numbers

The coordinates and the structure factors have been deposited in the Protein Data Bank (ID codes: 2E21 for TilS/AMPPNP, and 2E89 for TilS/ATP/Mg/Lys).